Radiation-induced amorphization of rare-earth titanate pyrochlores

Jie Lian, Jian Chen, L. M. Wang, and Rodney C. Ewing*
Department of Nuclear Engineering & Radiological Sciences, University of Michigan, Ann Arbor, Michigan 48109-2104, USA

J. Matt Farmer and Lynn A. Boatner
Solid State Division, Oak Ridge National Laboratory, Oak Ridge, Tennessee 37831-6056, USA

K. B. Helean
Department of Chemical Engineering and Materials Science, The University of California, Davis, California 95616, USA
(Received 12 November 2002; revised manuscript received 23 May 2003; published 15 October 2003)

Single crystals of the entire series of $A_2Ti_2O_7$ (A=Sm to Lu, and Y) pyrochlore compounds were irradiated by 1-MeV Kr^+ ions at temperatures from 293 to 1073 K, and the microstructure evolution, as a function of increasing radiation fluence, was characterized using *in situ* transmission electron microscopy (TEM). The critical amorphization temperature, T_c, generally increases from ~480 to ~1120 K with increasing A-site cation size (e.g., 0.977 Å for Lu^{3+} to 1.079 Å for Sm^{3+}). An abnormally high susceptibility to ion beam damage was found for $Gd_2Ti_2O_7$ (with the highest T_c of ~1120 K). Factors influencing the response of titanate pyrochlores to ion irradiation-induced amorphization are discussed in terms of cation radius ratio, defect formation, and the tendency to undergo an order-disorder transition to the defect-fluorite structure. The resistance of the pyrochlore structure to ion beam-induced amorphization is not only affected by the relative sizes of the A- and B-site cations, but also the cation electronic configuration and the structural disorder. Pyrochlore compositions that have larger structural deviations from the ideal fluorite structure, as evidenced by the smaller 48f oxygen positional parameter, x, are more sensitive to ion beam-induced amorphization.

DOI: 10.1103/PhysRevB.68.134107 PACS number(s): 61.82.−d, 61.80.Jh, 81.40.Wx, 72.80.Ng

I. INTRODUCTION

The pyrochlore structure $A_{1-2}B_2O_6Y_{0-1}$ encompasses a wide range of chemistries that are manifested by over 450 known synthetic compositions.[1,2] The pyrochlore structure-type is a derivative of the fluorite structure, AX_2, but with two cation sites and one-eighth fewer anions. The larger A^{3+} cation is eight-coordinated and located within a distorted cubic coordination polyhedron; the smaller B^{4+} cation is six-coordinated in a distorted octahedron. There are two unique oxygen sites: the 48f oxygen is coordinated to two B^{4+} cations and two A^{3+} cations, while the 8b oxygen is in a tetrahedral coordination with only A^{3+} cations. An unoccupied interstitial site, 8a, is surrounded by four B^{4+} ions, and the ''vacancies'' at the 8a site are ordered on the anion sublattice (see Ref. 3).[1–3] The pyrochlore structure is completely described by the cubic lattice parameter, **a**, and the 48f oxygen positional parameter, x (see Ref. 2). When actinides are substituted into the pyrochlore structure, they preferentially occupy the A site.[4] As a result, pyrochlores are important ceramic waste forms for actinide immobilization[5] and are among the principal host phases currently considered for the disposition of Pu from dismantled nuclear weapons.[6]

Naturally occurring pyrochlores are often found in the aperiodic, metamict state due to radiation damage from α-decay events of nuclides in the decay series of ^{238}U, ^{235}U, and ^{232}Th.[7] Synthetic $Gd_2Ti_2O_7$ doped with ^{244}Cm is very susceptible to α-decay damage and transforms to an amorphous structure after a dose of 2.3×10^{25} α-decays/m^3.[8] This amorphization process leads to a factor of 50 increase in the Pu-release rate.[8] *In situ* transmission electron microscopy (TEM) during ion irradiation[9] shows that $Gd_2Ti_2O_7$ is readily amorphized at a relatively low dose (~0.18 dpa) by 1-MeV Kr^+ irradiation—i.e., at a value that is consistent with the dose (~0.16 dpa) received by ^{244}Cm-doped $Gd_2Ti_2O_7$.[6,8] However, a study of $Gd_2Ti_{2-x}Zr_xO_7$ showed a systematic increase in the resistance to ion-beam-induced amorphization with increasing zirconium content in the B site,[10,11] and the end-member pyrochlore $Gd_2Zr_2O_7$ remained crystalline at a dose of ~36 dpa under 1.5-MeV Xe^+ irradiation at T=25 K.[12] This high ''resistance'' of zirconate compounds to ion-beam-induced amorphization has been also confirmed by Sickafus *et al.* for $Er_2Zr_2O_7$.[13] In contrast to the ordered pyrochlore $Er_2Ti_2O_7$, $Er_2Zr_2O_7$, which adopts a defect-fluorite structure, readily accommodates structural disordering and remains crystalline at a high dose of ~140 dpa (5×10^{16} ions/cm^2 by 350-keV Xe^+ at room temperature).

Recently, there have been an extensive series of simulations employing energy minimization and modern potential methods what have focused on the calculation of defect formation energies in pyrochlores of different compositions.[14–16] These studies were directed toward achieving an increased understanding of the observed greater radiation stability of Zr-rich pyrochlores and the effects of various cation substitutions at the A and B sites. There are significant discrepancies among the simulation results due to variations in the potentials employed, (e.g., for $La_2Zr_2O_7$, the predicted cation antisite formation energy is 1.95 eV,[16] whereas the value determined by Minervini *et al.*[14] is 4.4–4.8 eV). The general trend, however, is consistent, i.e., the cation antisite is the most stable defect in the pyrochlore structure and has the lowest energy of formation. The antisite defect formation energy is usually determined by the cation

ionic radius ratio, r_A/r_B, and the structure is predicted to become increasingly more radiation ''tolerant'' as the ionic radius of the *A*-site cation approaches that of the *B*-site cation. This is consistent with the prior radiation-damage results[10] for the $Gd_2Zr_xTi_{2-x}O_7$ system, where the radiation ''resistance'' to ion-beam-induced amorphization increased with the increasing average *B*-site cation size from $Gd_2Ti_2O_7$ to the end member $Gd_2Zr_2O_7$. Although the simulations correctly predict the effect of the *B*-site cation on the relative resistance to radiation-induced amorphization, several aspects remain unresolved. First, the effects of dynamic annealing at elevated temperatures on the radiation-induced amorphization have not been accounted for in the simulations. Therefore, the critical temperature at which the crystalline structure persists cannot be predicted. Second, the effects of *A*-site cations (e.g., variations in ionic radius, bond-type and electronic configuration) on the radiation damage and annealing process have not been explained. A significantly different radiation behavior within the stoichiometric zirconate pyrochlores has previously been observed, and in contrast to $Gd_2Zr_2O_7$, $La_2Zr_2O_7$ can be amorphized at room temperature at a dose of ~5.5 dpa.[12] Third, the simulations deal mainly with the defect formation energy; however, the more important phenomenon in the damage process, i.e., defect migration and recombination, have not been simulated.

Wang *et al.*[17] studied ion-beam-induced amorphization in the polycrystalline pyrochlores, $A_2Ti_2O_7$ (A=Gd, Eu, Sm, Y), using a 1-MeV Kr^+ irradiation. The critical amorphization temperatures, T_c, have been determined to be 1100, 1080, 1060, and 780 K for Gd-, Eu-, Sm-, and Y-titanate pyrochlores. This result indicated that the responses of titanate pyrochlores to ion beam induced-amorphization vary with different lanthanide ions occupying an *A* site. However, a previous study[18] reported a similar critical amorphization temperature (~975 K) for $A_2Ti_2O_7$ (A=Y, Sm, Gd, and Lu) under a 600-keV Bi^+ ion irradiation by *in situ* TEM observations, suggesting no significant effects of *A*-site cations on the resistance of titanate pyrochlores to ion-beam-induced amorphization. However, the contribution from the unaffected crystalline matrix beyond the ion range is difficult to avoid during the *in situ* TEM experiments due to the limited ion range (~60 nm) of the 600-keV Bi^+ in titanate pyrochlores. In the present study, we have synthesized single crystals of the rare-earth titanate pyrochlore, $A_2Ti_2O_7$ (A=Sm to Lu, and Y), and investigated the ion irradiation effects using 1.0-MeV Kr^+ ions over the temperature range of 293–1073 K. The microstructure evolution during ion irradiation has been characterized by *in situ* TEM techniques, and the effects of material properties (i.e., cation ionic size, electronic configuration and structural deviation) on the response of titanate pyrochlores to ion-beam-induced amorphization have been discussed.

II. EXPERIMENT

A. Crystal growth

Single crystals of $A_2Ti_2O_7$ (A=Sm to Lu, and Y) were grown at T=1508 K in a molten mixture consisting of the specific rare-earth oxide (RE_2O_3), titanium oxide (TiO_2), and lead fluoride (PbF_2). The technique required the slow evaporation of the flux (PbF_2) during the five-day high temperature synthesis period. Excess PbF_2 flux that remained primarily on the surface of the crystals was removed physically before analysis. The growth process was completed in air in a Pt crucible placed in a temperature-programmable furnace employing SiC heating elements.

B. Single crystal x-ray diffraction

Single-crystal x-ray diffraction measurements were performed using an Enraf-Nonius CAD4-F autodiffractometer employing Mo K_α radiation (λ=0.71073 Å). All of the data were collected in the ω-2θ mode at a varied scan rate of 0.54–5.17 min^{-1} and in the range of 3.0–56.0° (*h*: 0–10; *k*: 0–10; *l*: 0–10). The data were corrected for Lorentz and polarization effects after which absorption corrections were applied. The initial atomic positions for the refinement were taken from the work of Knop *et al.*[19] All of the atoms were refined anisotropically using the full-matrix, least-squares procedure.[20] Final residual density maps revealed some density in the vicinity of the metal ions.

C. Ion irradiation and *in situ* TEM observation

Ion irradiation and *in situ* TEM observations were performed using the IVEM-Tandem Facility at the Argonne National Laboratory over the temperature range of room temperature to 1073 K using 1-MeV Kr^+ ions. A constant ion flux of 6.25×10^{11} ions/cm^2 was used for the ion irradiations. Using the SRIM-2000 code,[21] the calculated ~300-nm range of the 1-MeV Kr^+ ions is greater than the typical sample thickness (~200 nm) suitable for TEM observation.[22] Most of 1-MeV Kr^+ ions, therefore, pass through the sample thickness examined, and ion-implantation effects are negligible. During irradiation, the ion beam was aligned approximately normal to the sample surface. To avoid concurrent electron beam irradiation damage, the electron beam was turned off during the ion irradiation. The crystalline-to-amorphous transformation was monitored intermittently by selected-area electron diffraction (SAED) patterns. The critical amorphization fluence (D_c), at which complete amorphization occurs, was experimentally determined by the disappearance of all of the diffraction maxima in the SAED patterns. The critical amorphization fluence has been converted into a unit of displacements per atom (dpa) using SRIM-2000 simulations with a displacement energy of 50 eV for all of the titanate pyrochlores.

III. RESULTS AND DISCUSSION

A. Structure refinements

The structural parameters of the rare-earth titanate pyrochlores as obtained from refinements of the single crystal x-ray diffraction data are summarized in Table I. The values of the cubic lattice parameters are in reasonable agreement with the values reported earlier by Subramanian *et al.*[1] and show an approximately linear relationship to the changing *A*-site cation ionic radius[23] (Fig. 1). The solid-state chemistry

TABLE I. Structural parameters (Å) of rare-earth titanate pyrochlores obtained from single crystal x-ray diffraction refinements. Errors are reported in parentheses.

composition	A^{3+} ionic radius (Ref. 23)	r_A/r_B	lattice parameter	$O_{48f}x$ parameter	$\langle A\text{-}O_{8b}\rangle$ bond length	$\langle A\text{-}O_{48f}\rangle$ bond length	$\langle \text{Ti-}O_{48f}\rangle$ bond length
$Sm_2Ti_2O_7$	1.079	1.78	10.2056(6)	0.3270(8)	2.210(1)	2.524(4)	1.968(2)
$Eu_2Ti_2O_7$	1.066	1.76	10.1943(9)	0.3267(3)	2.207(2)	2.523(2)	1.965(2)
$Gd_2Ti_2O_7$	1.053	1.74	10.1860(2)	0.3263(6)	2.205(1)	2.524(4)	1.961(3)
$Tb_2Ti_2O_7$	1.04	1.72	10.1589(6)	0.3281(5)	2.199(1)	2.505(1)	1.963(2)
$Dy_2Ti_2O_7$	1.027	1.70	10.1240(3)	0.3275(5)	2.192(1)	2.503(3)	1.953(2)
$Y_2Ti_2O_7$	1.019	1.68	10.1002(6)	0.3300(4)	2.187(1)	2.477(3)	1.960(2)
$Ho_2Ti_2O_7$	1.015	1.68	10.1041(2)	0.3285(5)	2.187(1)	2.489(4)	1.954(2)
$Er_2Ti_2O_7$	1.004	1.66	10.0787(3)	0.3278(8)	2.182(1)	2.488(6)	1.946(3)
$Tm_2Ti_2O_7$	0.994	1.64	10.0638(5)	0.3292(3)	2.179(1)	2.474(3)	1.950(1)
$Yb_2Ti_2O_7$	0.985	1.63	10.0325(3)	0.3309(4)	2.192(1)	2.503(3)	1.953(1)
$Lu_2Ti_2O_7$	0.977	1.61	10.0172(4)	0.3297(11)	2.169(1)	2.459(7)	1.943(4)

of the lanthanide atoms in combination with oxygen is primarily dependent on the ionic size and the electronic configuration. In the lanthanides, as electrons are added to the $4f$ orbital with the increasing atomic number from La to Lu, the electrons in the $4f$ orbital are effectively shielded by the outer shell of $5d^1$ and $6s^2$ valence electrons, which leads to the stable trivalent state for lanthanide ions.[24] Due to the predominance of ionic bonding between the lanthanide elements and oxygen, the cubic lattice parameter for single crystals of $A_2Ti_2O_7$ displays a nearly linear relation to the ionic radii.

The $48f$ oxygen positional parameter, x, varies from 0.3263 to 0.3309 over the series of titanate pyrochlores (Table I). A significant change in the x parameter for the rare-earth titanate pyrochlores is obtained by varying the ionic size of the A-site cation (Fig. 2). There is a general monotonic increase of the x positional parameter as the A-site cation radius decreases relative to the B^{4+} cation for stannate pyrochlores, as reported in a previous study.[25] For titanate pyrochlores, different methods have been used to determine the x parameter, including x-ray,[19] electron[26] and neutron diffraction,[19] as well as theoretical simulations.[27] The reported results, as shown in Fig. 2, are inconsistent in their absolute values.[28,29] Tabira *et al.*[26] reported a systematic change with the rare-earth ion size of the x parameter using wide-angle convergent-beam electron diffraction for a series of titanate and zirconate pyrochlores. However, the relative intensity of CBED is sensitive to sample thickness variation, and the variation in dynamic effects of electron diffraction with various sample thicknesses could affect significantly the accuracy of measured x values. Minervini *et al.*[27] predicted a decrease of x parameter with the increasing A-site cation ionic radii based on the energy minimization method. In their simulation, a significant underestimation of the x value was found, as compared with the experimental results. Furthermore, the same disordering formation energy was used for all pyrochlore compounds. In such a case, it is difficult to predict the degree of structural disorder, e.g., for $Gd_2Ti_2O_7$; the degree of oxygen disordering determined by Minervini *et al.* (0.17%) is much higher than the experimental value (0.01%) reported by Tuller.[30]

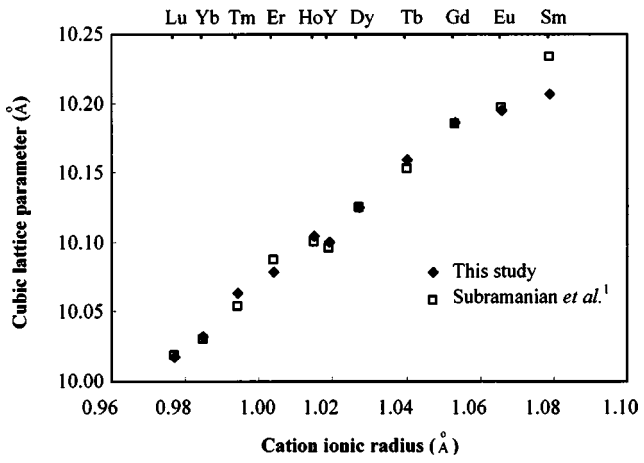

FIG. 1. The isometric lattice parameter for the rare-earth series of titanate pyrochlore compositions as determined by single crystal x-ray diffraction refinements.

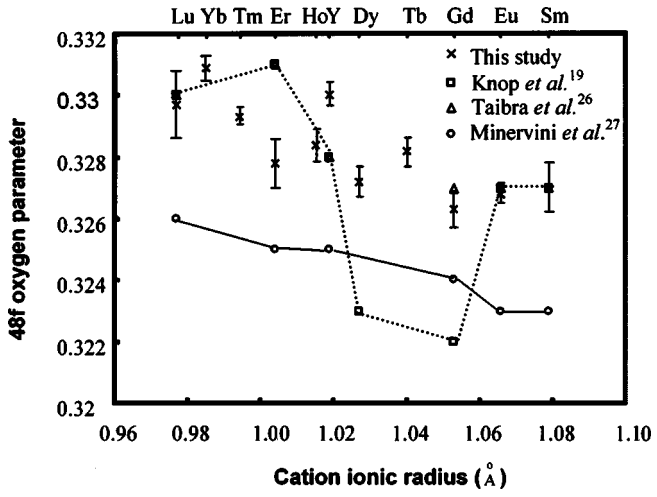

FIG. 2. The $48f$ oxygen positional parameter, x, of titanate pyrochlores obtained from single-crystal structural refinements. The smallest x value is for $Gd_2Ti_2O_7$.

In addition to the cation size effect, the x values for pyrochlores could be affected by residual structural disorder. It is expected that varying degrees of disorder could occur in some compositions. However, the intrinsic cation and anion disorder for titanate pyrochlores is very low (e.g., the anion disorder is 0.01% for $Gd_2Ti_2O_7$) because of the specific ion size and valence state constraints on the formation of the pyrochlore superstructure. This is also evident from the fact that no thermally induced order-disorder structural transformation occurs for titanate pyrochlores upon heating. In the present investigation, the variation in the x values is relatively consistent with that reported by Knop *et al.*[19] based on an x-ray structure refinement on powdered samples (see Fig. 2). The difference in the absolute x values obtained by single crystal refinements, as compared to Knop *et al.*'s data, could be caused by the different experimental methods employed in the determination of x values. For both studies, $Gd_2Ti_2O_7$ has the smallest x value. This is inconsistent with the expected trend of the x parameter increasing as a function of decreasing ion size, suggesting that other factors play an important role in determining the oxygen positional parameter. Cation electronic configurations and the metal-oxygen bond character change the cation polyhedral geometry and degree of structural distortion, and as a result, may have a significant effect on the x parameter. There is a strong hybridization of the Ti $3d$ and O $2p$ valence state for rare-earth titanate pyrochlores, and it is this interaction that is responsible for the chemical bonding in the distorted Ti-O_{48f}octahedron.[31] An increasing overlap of the Ti $3d$ and O $2p$ orbital occurs in $A_2Ti_2O_7$ as one goes from Sm or Lu toward a maximum at Gd. This increasing Ti-O_{48f} overlap is also evidenced by the relatively shorter bond distances of $\langle$Ti-$O_{48f}\rangle$ for the Gd- and Dy-titanate pyrochlores (Table I). Furthermore, the O $1s$ binding energy for $Gd_2Ti_2O_7$ is the lowest among the $A_2Ti_2O_7$ pyrochlore compositions, which also confirms the increasing Ti-O_{48f} overlap in $Gd_2Ti_2O_7$. Nemoshkalenko *et al.*[32] also observed an anomalous build-up of electron density on the O_{48f} atoms in $Gd_2Ti_2O_7$. The increasing Ti $3d$ and O $2p$ orbital overlap leads to the lower oxygen positional parameter x for $Gd_2Ti_2O_7$ and $Dy_2Ti_2O_7$. Furthermore, Gd^{3+} and Lu^{3+} have a strong ionic character when bound to oxygen due to the specific electronic configuration of the $4f$ subshell for Gd^{3+} (half-filled) and Lu^{3+} (filled). This displaces the oxygen atoms toward the Ti^{4+}, which causes a further decrease in the oxygen positional parameter x for $Gd_2Ti_2O_7$ and $Lu_2Ti_2O_7$, as compared with the nearby rare-earth titanate pyrochlores. The large x value found for $Y_2Ti_2O_7$ in this study can be related to the high level of residual disordering that accompanies the Y-Ti substitution—as revealed by a neutron diffraction refinement.[33]

B. Ion-irradiation-induced amorphization and temperature dependence

All of the titanate pyrochlores were readily amorphized by a 1-MeV Kr^+ ion irradiation at room temperature. The characteristic microstructure evolution due to increasing levels of radiation damage (i.e., the gradually decreasing intensity of the diffraction maxima, and the appearance of an amorphous halo with increasing ion dose.) was observed by *in situ* TEM (Fig. 3). Above the critical amorphization dose D_c, diffraction maxima from the crystalline domains disappear completely, and the final fully amorphous state was achieved as revealed by the SAED patterns. The temperature dependences of the critical amorphization fluence for the titanate pyrochlores irradiated by 1-MeV Kr^+ ions are shown in Fig. 4. For all of the titanate pyrochlores, the critical amorphization fluence increases with increasing temperature due to dynamic annealing effects. Above a critical amorphization temperature, T_c, the critical amorphization fluence increases to infinity, and complete amorphization does not occur.

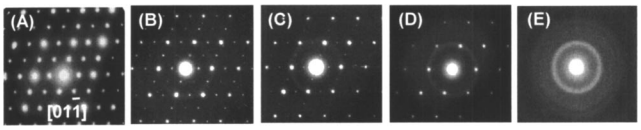

FIG. 3. A sequence of selected area diffraction patterns for $Lu_2Ti_2O_7$ irradiated by 1-MeV Kr^+ ions at room temperature: (a) original; (b) 0.937×10^{14} ions/cm^2 ($\sim$0.12 dpa); (c) 1.562×10^{14} ions/cm^2 ($\sim$0.19 dpa); (d) 2.812×10^{14} ions/cm^2 ($\sim$0.33 dpa); (e) 4.063×10^{14} ions/cm^2 ($\sim$0.55 dpa).

Different mechanisms are proposed to describe the ion irradiation-induced amorphization process. The amorphization may occur when the accumulation of defects created by ion irradiation exceeds the critical concentration necessary for amorphization due to the overlap of collision cascades.[34–36] Furthermore, direct impact amorphization has been considered to be one of the fundamental amorphization mechanisms for complex ceramics under heavy-ion irradiations.[34,37] For the pyrochlore structure, it is not clear whether the direct impact or defect accumulation mechanisms control the ion-irradiation-induced amorphization process. An *ex situ* high-resolution TEM image of $Gd_2Ti_2O_7$ irradiated by 1.5-MeV Xe^+ from a previous study shows

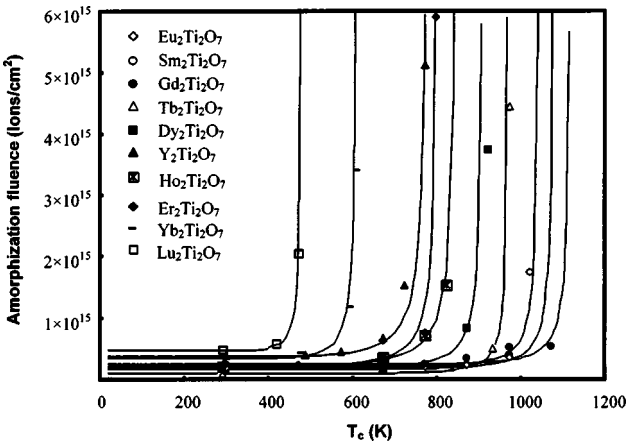

FIG. 4. Temperature dependence of the critical amorphization fluence of rare-earth titanate pyrochlores under 1-MeV Kr^+ ion irradiation. The critical amorphization temperature, T_c, and activation energy, E_a, for dynamic defect annealing were determined from these data based on a cascade-quenching model (see Table II) (Ref. 37).

TABLE II. The critical amorphization temperature, T_c, activation energy of defect annealing, E_a, and critical dose at 293 K for each rare-earth titanate pyrochlore. These values were determined based on a cascade-quench model.[37] The ion range and number of displacements per ion were calculated by SRIM-2000. The energy deposition by nuclear collision and electron ionization processes were calculated at the same position (~100 nm) as the amorphization dose, D_c, at room temperature.

composition	radius (Å)	r_A/r_B	density (g/cm^3)	ion range (nm)	vacancy per ion	dE/dx_e eV/nm/ion	dE/dx_n eV/nm/ion	ENSP	D_c at 293 K (dpa)	E_a (eV)	T_c (K)	$O_{48f}x$ parameter
$Sm_2Ti_2O_7$	1.079	1.78	6.357	292.6	3588	2170	1750	1.24	0.25	0.8	1045	0.3270(8)
$Eu_2Ti_2O_7$	1.066	1.76	6.418	290.3	3661	2170	1730	1.254	0.23	0.7	1080	0.3267(3)
$Gd_2Ti_2O_7$	1.053	1.74	6.567	267.9	3657	2140	1750	1.223	0.18	1	1120	0.3263(6)
$Tb_2Ti_2O_7$	1.04	1.72	6.662	266.5	3650	2170	1750	1.223	0.11	0.5	970	0.3281(5)
$Dy_2Ti_2O_7$	1.027	1.70	6.823	266.9	3805	2140	1770	1.209	0.25	0.5	910	0.3275(5)
$Y_2Ti_2O_7$	1.019	1.68	4.987	320.6	3595	1990	1640	1.213	0.37	0.4	780	0.3300(4)
$Ho_2Ti_2O_7$	1.015	1.68	6.926	263.9	3807	2130	1780	1.213	0.27	0.3	850	0.3285(5)
$Er_2Ti_2O_7$	1.004	1.66	7.039	277.2	3744	2220	1820	1.212	0.25	0.3	804	0.3278(8)
$Yb_2Ti_2O_7$	0.985	1.63	7.113	270.9	3710	2340	1950	1.20	0.45	0.45	611	0.3309(4)
$Lu_2Ti_2O_7$	0.977	1.61	7.288	274	3750	2270	1900	1.195	0.55	0.6	480	0.3297(11)

evidence of cascade-quenching features in heavy-ion irradiated pyrochlore compounds.[9] Based on the direct-impact model, a highly energetic incident ion transfers its kinetic energy to the target within 10^{-13} sec, and creates a displacement cascade, typically a few nanometers in size. This highly energetic zone quenches quickly (within a few picoseconds) to form a small amorphous domain. Epitaxial recrystallization may occur at the amorphous/crystalline interface.[38] With increasing ion dose, the accumulation and overlap of the small amorphous domains eventually leads to complete amorphization.

The temperature dependence of the amorphization fluence, D_c, can be expressed by[37,39]

$$D_c = \frac{D_0}{1-\exp[(E_a/k)(1/T_c)-(1/T)]}, \quad (1)$$

where D_0 is the amorphization fluence extrapolated to absolute zero—the point at which no annealing can occur. E_a is the activation energy for the dynamic annealing process during irradiation; T_c is the critical amorphization temperature above which the recrystallization rate is greater than the amorphization rate, and complete amorphization does not occur. Details on the temperature dependence of materials to ion beam-induced amorphization have been previously discussed (see Refs. 9, 17, 37, and 38). Based on Eq. (1), the critical amorphization temperature, T_c, and the activation energy of recrystallization, E_a, can be determined (Table II). However, the calculated activation energy is strongly dependent on the model used to fit the curve of the temperature dependence of the critical amorphization fluence (Fig. 4), and significant uncertainty can be induced depending on the damage accumulation model that is used.[40] Thus, these calculated activation energies are less useful than the critical amorphization temperature, T_c, in evaluating a material's ''susceptibility'' to radiation-induced amorphization.

Generally, the critical amorphization temperature is dependent on both the properties of the material (e.g., chemical composition and structure) and irradiation conditions (e.g., incident ion species, target atom mass and damage rate).[40,41] In this study, we have used a constant ion flux during 1-MeV Kr^+ ion irradiations for all of the titanate pyrochlores, which allows us to compare the radiation response of the different titanate pyrochlore compositions to ion-beam-induced amorphization. However, the differences in composition and density may affect the electronic to nuclear stopping power ratio (ENSP) and the rate of energy deposition, which slightly impact the critical amorphization temperature. Meldrum *et al.*[40] have shown that electron irradiations can enhance defect recombination and induce crystallization as a result of ionization processes in amorphous orthophosphates. The electronic-to-nuclear stopping power ratio (ENSP) correlates well with the critical amorphization temperatures for zircon structure-type APO_4 (A=Sc, Y, Tb, Tb, Tm, and Lu) and monazite structure-type APO_4 (A=La, Pr, Nd, Sm, Eu, and Gd). We have performed the full cascade calculations using the SRIM-2000 code with displacement energies of 50 eV for all of the irradiated titanate pyrochlore compounds. The calculated ion range, damage events, the energy deposited by nuclear collision (dE/dx_n) or electron ionization process (dE/dx_e) have been tabulated in Table II. The energy deposition is calculated under the same condition and at the same depth (~100 nm) as the amorphization dose. No significant variations in energy deposition by nuclear collision or electron ionization processes have been found for all of titanate pyrochlore compounds, except for $Y_2Ti_2O_7$. Furthermore, the ENSP (~1.2) is similar for all titanate pyrochlores. These calculations suggest that irradiation conditions do not have a significant effect on the determination of critical amorphization temperatures for titanate pyrochlores, and the very different behaviors under irradiation for $A_2Ti_2O_7$ pyrochlores with varying A-site cation compositions from Lu^{3+} to Sm^{3+} (Fig. 4) are closely correlated to the properties of the material (e.g., cation size, deviation from the ideal structure and distortion of coordination polyhedra, and defect migration).

The relationship between the critical amorphization temperature, T_c, of the $A_2Ti_2O_7$ pyrochlore single crystals under 1-MeV Kr^+ ion irradiation, and the A-site cation ionic radius is shown in Fig. 5. Similar critical amorphization tempera-

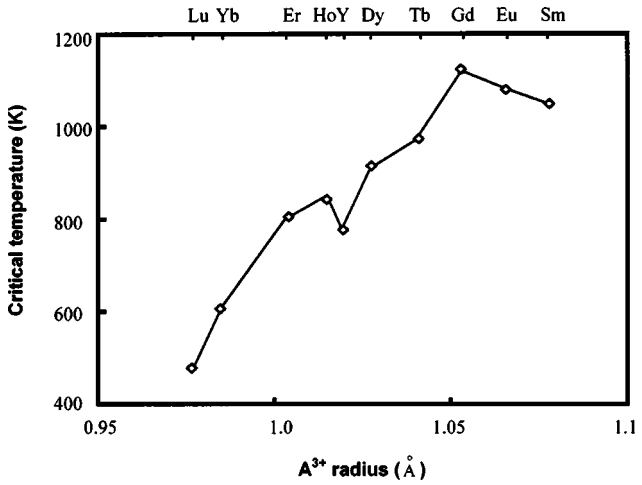

FIG. 5. The critical amorphization temperature, T_c, as a function of the *A*-site cation ionic radius.

tures, T_c, of titanate pyrochlores subjected to 1-MeV Kr^+ ion irradiations have been obtained for single crystals as compared to the limited data for polycrystalline samples. For example, the critical amorphization temperatures are 1120, 1080, and 1045 K for Gd-, Eu-, and Sm-titanate single crystals, respectively; while, the T_c of polycrystalline $Gd_2Ti_2O_7$,[9,10] $Eu_2Ti_2O_7$, and $Sm_2Ti_2O_7$ (Ref. 11) with 1-MeV Kr^+ ion irradiation are 1100, 1080, and 1060 K. A similar radiation response of single crystals and polycrystalline samples is expected given that the chemical compositions and experimental conditions are the same. Generally, as the ionic radius of lanthanide cations increases from Lu^{3+} to Gd^{3+}, the critical amorphization temperature, T_c, increases continuously except for $Y_2Ti_2O_7$. As the ionic radius increases from Gd^{3+} to Sm^{3+}, the critical temperature, T_c, decreases. The highest critical temperature ($\sim$1120 K) is for $Gd_2Ti_2O_7$, and this is inconsistent with the general trend expected based on the ionic radius. There are other examples of anomalous behavior of Gd-compounds as compared with analogous lanthanide compounds. For example, an abnormally high solidification temperature was observed for Gd_2O_3,[42] which is typically attributed to the specific electronic state of Gd^{3+} with the half-filled $4f$ subshell ($4f^7$). Furthermore, the highest ionic conductivity is observed for $Gd_2Ti_2O_7$ within the Ca-doped $A_2Ti_2O_7$ pyrochlores (A = Sm, Y, Gd).[43]

The slight deviation from the monotonic trend of T_c versus the ionic radius exhibited by $Y_2Ti_2O_7$ may be attributed to its slightly lower sensitivity to ion-beam damage, in which fewer displacements are created by each incident ion due to the lower target density of $Y_2Ti_2O_7$ as compared with the other titanate pyrochlores. Due to a lower damage production rate, as compared to that of the nearby chemical compositions, a slightly lower critical amorphization temperature is expected for $Y_2Ti_2O_7$.

C. Order-disorder transition and radiation "resistance"

An ion-irradiation-induced order-disorder transformation has been observed in all of the irradiated titanate pyrochlores. For $Gd_2Ti_2O_7$, the ion-irradiation-induced order-disorder transformation occurs concurrently with the amorphization process. In this case, the diffraction maxima from the superstructure of the ordered-pyrochlore phase disappeared with the appearance of the diffuse diffraction halos (characteristic of amorphous domains). A defect-fluorite layer forms at the outer edge of the displacement cascade by disordering the *A*- and *B*-site cations during the process of epitaxial recrystallization. This ion-irradiation-induced defect structure is susceptible to further radiation damage at room temperature. With increasing ion dose, the defect fluorite structure of $Gd_2Ti_2O_7$ is completely amorphized ($\sim$0.18 dpa). In the case of $Lu_2Ti_2O_7$, this irradiation-induced pyrochlore-fluorite structural transformation is almost complete prior to the appearance of the diffuse halos at room temperature [Fig. 4(c)]. In contrast to the radiation damage-resistant defect fluorite structure of irradiated $Gd_2Zr_2O_7$, we observed that the defect-fluorite structure in $Lu_2Ti_2O_7$ was unstable relative to the amorphous state under irradiation at room temperature, and the fully amorphous state was achieved at a critical amorphization dose of $\sim$0.55 dpa.

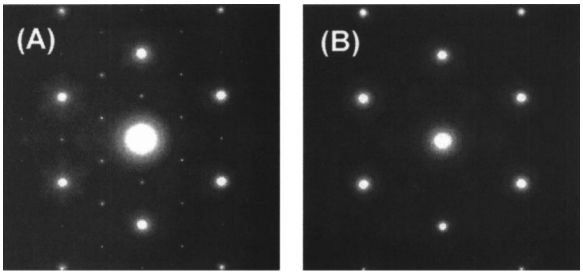

FIG. 6. SAED diffraction patterns of $Er_2Ti_2O_7$ irradiated by 1-MeV Kr^+ at 873 K, slightly above the critical amorphization temperature: (A) original; (B) 1.8×10^{14} ions/cm^2 ($\sim$0.21 dpa). The defect fluorite structure was stable relative to the fully amorphous state.

At a higher ambient temperature, for which the recrystallization efficiency is higher, the entire cascade is fully recrystallized to a disordered-fluorite structure. In this case, the ion irradiation-induced defect fluorite structure is stable under further irradiation without amorphization. This condition can be reached at or slightly above the critical amorphization temperature. The ion irradiation-induced defect fluorite persisted with no evidence of amorphization in $Er_2Ti_2O_7$ irradiated by 1-MeV Kr^+ at a fluence of 1.87×10^{14} ions/cm^2 ($\sim$0.21 dpa) at 873 K, slightly above T_c (Fig. 6). This demonstrates that the stability of the defect-fluorite created by ion irradiation in pyrochlore compounds can be estimated by a consideration of the critical amorphization temperature. For $Lu_2Ti_2O_7$, the ion-irradiation-induced defect-fluorite structure is stable above 480 K, while the defect-fluorite structure of $Gd_2Zr_2O_7$ persists with respect to the amorphous state down to $T=25$ K. As the ionic radius of the *A*-site cation approaches that of the *B*-site cation, the pyrochlore structure shows a greater tendency to transform to a defect-fluorite structure under ion irradiation, and the ion-irradiation-induced defect-fluorite structures are increasingly stable. These results allow us to correlate the "resistance" to

ion-beam-induced amorphization of pyrochlore compounds with the crystal chemistry and its tendency toward an order-disorder transition.

For the ordered pyrochlore, $A_2B_2O_7$, the phase stability of the superstructure is basically determined by the *A*- and *B*-site cation radius ratio. The systematic decrease in the average *A*- to *B*-site cation radius ratio leads to a gradual disordering of the pyrochlore structure to an anion-deficient fluorite structure $(A, B)_4O_7$.[44] An upper radius ratio also exists, above which the cubic pyrochlore cannot form. This cation ionic radius ratio for the stable phase of the ordered pyrochlore has been determined to lie between 1.46 ($Gd_2Zr_2O_7$) and 1.78 ($Sm_2Ti_2O_7$).[1]

The cation radius ratio has also been used to predict the stability of pyrochlores under heavy-ion irradiation.[13] Energy-minimization calculations[14,45] have suggested that the cation antisite defect is the most stable defect in the pyrochlore structure. As the *A*-site cation radius approaches the *B*-site cation radius, the material has a higher capacity for accommodating the antisite cation defect; and thus, a low cation ionic radius ratio energetically favors a disordered structure by reducing the defect formation energy. The defect-formation energy has a significant effect on the susceptibility of the structure to radiation damage. Under irradiation, the lattice energy increases rapidly—especially in materials with a high defect formation energy. When the free energy of the crystalline structure during irradiation is greater than the free energy of the aperiodic state, the material is more easily amorphized.[45]

Energy-minimization calculations[13,14,45] predict similar cation antisite defect formation energies and a similar extent of structural disorder for all of the titanate pyrochlores, suggesting a similar radiation response behavior. However, an obvious difference in the susceptibility to ion beam-induced amorphization was found for the titanate pyrochlores with different *A*-site cations under the same irradiation conditions (1-MeV Kr^+ ion irradiation; see Fig. 4). Furthermore, based on the cation radius ratio, a monotonic increase of resistance to ion beam-induced amorphization is expected as the cation radius ratio decreases from 1.78 ($Sm_2Ti_2O_7$) to 1.61 ($Lu_2Ti_2O_7$). However, for the titanate pyrochlores, $A_2Ti_2O_7$ (A=Sm-Lu), the critical amorphization temperatures, T_c, increase from Lu to Gd and decrease from Gd to Sm. The highest critical temperature is for $Gd_2Ti_2O_7$, suggesting a higher susceptibility to amorphization than that of other $A_2Ti_2O_7$ pyrochlore compositions.

The observation that $Gd_2Ti_2O_7$ has the highest critical amorphization temperature among the titanate compositions is of particular interest. This failure of the cation radius-ratio criteria has also been reported in a previous study,[46] where the +2, +5 pyrochlore $Cd_2Nb_2O_7$ showed a much different behavior under radiation than the +3, +4 pyrochlore $Gd_2Ti_2O_7$, although both pyrochlores have a similar cation radius ratio ($r_{Cd}/r_{Nb}=1.72:1, r_{Gd}/r_{Ti}=1.74:1$). The issue for the cation-radius-ratio criteria is whether similar *A*- and *B*-site cation radii really induce structural disordering and reduce the defect formation energy. Stannate pyrochlores such as $Y_2(Sn_xTi_{1-x})_2O_7$ and $Gd_2(Sn_xTi_{1-x})_2O_7$ illustrate the limitations of this criterion. Rietveld x-ray analysis and neutron powder diffraction have indicated that a substitution of the larger Sn^{4+} ion for Ti^{4+} does not induce structural disorder.[47] This is probably due to the strongly covalent Sn^{4+}-O bonds. Thus, the relative ionic radius ratio alone and calculated defect formation energies cannot generally or accurately predict the extent of structural disorder or the radiation resistance of different pyrochlore compositions.

An ordered pyrochlore structure can be described by the cubic lattice parameter, ***a***, and the 48 *f* oxygen positional parameter, *x*.[1,2] Due to the oxygen vacancy at the 8*a* site, surrounded by four B^{4+} cations in the ordered pyrochlore structure, the electrostatic repulsion between exposed *B*-site cations is compensated by the displacement of the 48*f* oxygen towards the exposed *B*-site cations. The parameter *x* of the 48*f* oxygen defines the degree of distortion of the Ti-O octahedron, and the limiting values of *x* are 0.3125 and 0.375 for the pyrochlores. For $x=0.3125$, the *B*-site ions are in a perfect octahedral coordination and have a perfectly ordered pyrochlore structure. When $x=0.375$, the coordination polyhedron around *A* is a cube, and there is a complete disordering to the fluorite structure. Thus, the 48*f* oxygen *x* parameter can be used as a measure of the degree of structural disorder and the extent of deviation from the ideal fluorite structure. The variable 48*f* oxygen parameter, *x*, is an important measure of the tendency of the order-disorder transition for pyrochlore. For example, in zirconate pyrochlores, $A_2Zr_2O_7$, the pyrochlore-to-flu orite structural transformation can be induced by thermal treatment. The transition temperatures for $Nd_2Zr_2O_7$, $Sm_2Zr_2O_7$, and $Gd_2Zr_2O_7$ are 2573, 2473, and 1823 K, respectively. The increasing tendency at lower temperatures to an order-disorder transition is correlated with the increasing *x* parameter as compositions change from Nd- to Sm- to Gd-zirconate pyrochlores. This also suggests that the deviation from the ideal-fluorite structure determines the energetics of the order-disorder structural transition in different pyrochlore compositions.

Using *ab initio* methods, Chartier *et al.*[16] studied the influence of structural disordering and the order-disorder transition on the radiation resistance of the $La_2Ti_{2-x}Zr_xO_7$ system. They concluded that, under irradiation, cation disordering on the *A*- and *B*-sites becomes easier with an increase in the degree of cation disorder because it lowers the cation antisite formation energy, and the vacant oxygen 8*a* site becomes increasingly occupied. Combined with oxygen Frenkel pair formation, a significant portion of the kinetic energy of the energetic incident ions transferred by the ballistic process is dissipated by forming a disordered structure via cation antisite formation. In this case, the pyrochlore becomes more resistant to radiation-induced amorphization. This is consistent with a systematic radiation study of the $Gd_2Zr_xTi_{2-x}O_7$ system, where the pyrochlore compositions exhibited a gradually increasing resistance to ion irradiation-induced amorphization with increasing structural disordering to the defect-fluorite structure and a greater tendency toward an order-disorder transition at higher Zr-contents.

Based on the present results, one can account for the abnormally high susceptibility to amorphization for $Gd_2Ti_2O_7$ as illustrated in Fig. 5. $Gd_2Ti_2O_7$ has the smallest 48*f* oxygen positional parameter (0.3263), as compared to other rare-

earth titanate pyrochlores, suggesting the greatest deviation from the ideal fluorite structure. Therefore, $Gd_2Ti_2O_7$ exhibits the largest resistance to the pyrochlore-to-fluorite structural transformation, and, thus, has the highest susceptibility to ion-beam-induced amorphization. Furthermore, as shown in Fig. 5, we have observed the deviation from increasing susceptibility to amorphization for $Y_2Ti_2O_7$ from Lu- to Gd-titanate pyrochlores, which can be attributed to the slightly higher extent of residual disordering and a higher tendency toward the pyrochlore-to-fluorite structure transformation, as evidenced by the slightly larger *x* parameter for $Y_2Ti_2O_7$ than that of $Er_2Ti_2O_7$, $Ho_2Ti_2O_7$, and $Dy_2Ti_2O_7$.

Summarizing the analysis above, the deviation from the ideal fluorite structure and structural disordering, as reflected by the variation in 48*f* oxygen positional parameter, *x*, determines the energetics of the order-disorder transition, and correspondingly affects the susceptibility of pyrochlore to radiation-induced amorphization. The *x* parameter of different pyrochlore compositions is closely correlated with the cation size and electronic configuration. In general, the cation size factor is dominant in controlling the resistance of titanate pyrochlores to radiation-induced amorphization. However, the effect of the electronic configuration of the *A*-site cation must be considered, especially if the effects of the electronic configuration and cation sizes compensate one another. In the case of $Gd_2Ti_2O_7$, the Gd^{3+} electronic configuration and ⟨Ti-O⟩ bonding character may play important roles in determining the 48*f* oxygen parameter and the distortion of coordination polyhedra, which correspondingly affect the energetics of the order-disorder transition and the susceptibility of different pyrochlore compositions to radiation damage.

IV. CONCLUSIONS

Single-crystal rare-earth titanate pyrochlores $A_2Ti_2O_7$ (*A* = Sm to Lu, and Y) have been synthesized and their structures refined by single crystal x-ray diffraction analysis. Ion-irradiation experiments using 1-MeV Kr^+ ions were performed on the pyrochlores with *in situ* TEM observation. The effects of the properties of the material (e.g., cation size, electronic configuration, and the 48*f* oxygen *x* parameter) on the ''resistance'' of titanate pyrochlores to ion-beam-induced amorphization have been discussed. Major conclusions include:

(1) *A*-site cations have an important effect on the resistance of the pyrochlore structure type to ion-beam-induced amorphization. With increasing ionic radius from Lu^{3+} (0.977 Å) to Gd^{3+} (1.053 Å), the critical amorphization temperature increases from 480 to 1120 K, whereas, from Gd^{3+} to Sm^{3+}, the critical temperature decreases from 1120 to 1045 K. The highest critical amorphization temperature for $Gd_2Ti_2O_7$ suggests that this composition is more sensitive than other rare-earth titanate pyrochlores.

(2) A close correlation was found between the susceptibility of pyrochlore compositions to ion-beam-induced amorphization and the energetics of the order-disorder transition. Pyrochlores whose structure are closer to the ideal fluorite structure, which have the higher value for the 48*f* oxygen positional parameter, *x*, are energetically more susceptible to a pyrochlore-to-fluorite structural transition. Thus, pyrochlore compositions that are easily disordered to the defect-fluorite structure are more resistant to ion-beam-induced amorphization. Both the effects of cation size and electronic configuration must be considered in order to explain the response of rare-earth titanate pyrochlores to ion beam-induced amorphization.

ACKNOWLEDGMENTS

The authors thank the staff of the IVEM-Tandem Facility at the Argonne National Laboratory for assistance during ion irradiation experiments. This work was supported by the Office of Basic Energy Sciences, U.S. DOE, under DOE Grant No. DE-FG02-97ER45656. Oak Ridge National Laboratory is managed by UT-Battelle, LLC, for the U.S. DOE under Contract No. DE-AC05-00OR22725.

*Corresponding author. Electronic address: rodewing@umich.edu

[1] M. A. Subramanian, G. Aravamudan, and G. V. S. Rao, Prog. Solid State Chem. **15**, 55 (1983).
[2] B. C. Chakoumakos, J. Solid State Chem. **53**, 120 (1984).
[3] J. Lian, L. M. Wang, S. X. Wang, J. Chen, L. A. Boatner, and R. C. Ewing, Phys. Rev. Lett. **87**, 145901 (2001).
[4] B. C. Chakoumakos and R. C. Ewing, in *Scientific Basis for Nuclear Waste Management VIII*, edited by C. M. Jantzen, J. A. Stone and Rodney C. Ewing, MRS Symposia Proceedings No. 44 (Materials Research Society, Pittsburgh, 1985), p. 641.
[5] A. E. Ringwood, S. E. Kesson, N. G. Ware, W. Hibberson, and A. Major, Nature (London) **278**, 219 (1979).
[6] W. J. Weber and R. C. Ewing, Science **289**, 2051 (2000).
[7] G. R. Lumpkin and R. C. Ewing, Phys. Chem. Miner. **16**, 2 (1988).
[8] W. J. Weber, J. W. Wald, and Hj. Matzke, Mater. Lett. **3**, 173 (1985).
[9] S. X. Wang, L. M. Wang, R. C. Ewing, G. S. Was, and G. R. Lumpkin, Nucl. Instrum. Methods Phys. Res. B **148**, 704 (1999).
[10] S. X. Wang, B. D. Begg, L. M. Wang, R. C. Ewing, W. J. Weber, and K. V. G. Kutty, J. Mater. Res. **14**, 4470 (1999).
[11] S. X. Wang, L. M. Wang, R. C. Ewing, and K. V. G. Kutty, in *Microstructural Processes in Irradiated Materials*, edited by S. J. Zinkle, G. E. Lucas, R. C. Ewing, and J. S. Williams, MRS Symposia Proceedings No. 540 (Materials Research Society, Pittsburgh, 1999), p. 355.
[12] J. Lian, X. T. Zu, K. V. G. Kutty, J. Chen, L. M. Wang, and R. C. Ewing, Phys. Rev. B **66**, 054108 (2002).
[13] K. E. Sickafus, L. Minervini, R. W. Grimes, J. A. Valdez, M. Ishimaru, F. Li, K. J. McClellan, and T. Hartmann, Science **289**, 748 (2000).
[14] L. Minervini, R. W. Grimes, and K. E. Sickafus, J. Am. Ceram. Soc. **83**, 1873 (2000).
[15] R. E. Williford, W. J. Weber, R. Devanathan, and J. D. Gale, J. Electroceram. **3**, 409 (1999).
[16] A. Charties, C. Meis, W. J. Weber, and L. R. Corrales, Phys. Rev. B **65**, 134116 (2002).

[17] S. X. Wang, L. M. Wang, R. C. Ewing, and K. V. G. Kutty, Nucl. Instrum. Methods Phys. Res. B **169**, 135 (2000).
[18] B. D. Begg, N. J. Hess, W. J. Weber, R. Davanathan, J. P. Icenhower, S. Thevuthasan, and B. P. McGrail, J. Nucl. Mater. **288**, 208 (2001).
[19] O. Knop, F. Brisse, and L. Castelliz, C. R. Seances Acad. Sci., Ser. D **47**, 971 (1969).
[20] G. M. Sheldrick, SHEXLXL-97, University of Göttingen, Germany (1997).
[21] J. F. Ziegler, J. P. Biersack, and U. Littmark, *The Stopping and Range of Ions in Solids* (Pergamon, New York, 1985).
[22] L. M. Wang, Nucl. Instrum. Methods Phys. Res. B **141**, 312 (1998).
[23] R. D. Shannon, Acta Crystallogr., Sect. A: Cryst. Phys., Diffr., Theor. Gen. Crystallogr. **32**, 751 (1976).
[24] L. R. Morss, *Handbook on the Physics and Chemistry of Rare Earths* (North-Holland, Amsterdam, 1994), Vol. 18.
[25] B. J. Kennedy, B. A. Hunter, and C. J. Howard, J. Solid State Chem. **130**, 58 (1997).
[26] Y. Tabira, R. L. Withers, L. Minervini, and R. W. Grimes, J. Solid State Chem. **153**, 16 (2000).
[27] L. Minervini, R. W. Grimers, Y. Tibira, R. L. Withers, and K. E. Sickafus, Philos. Mag. A **82**, 123 (2002).
[28] R. A. McCauley, J. Appl. Phys. **51**, 290 (1980).
[29] Y. Calage and J. Pannetier, J. Phys. Chem. Solids **38**, 711 (1977).
[30] H. L. Tuller, J. Phys. Chem. Solids **55**, 1393 (1994).
[31] V. V. Nemoshkalenko, S. V. Borisenko, V. N. Uvarov, A. N. Yasesko, A. G. Vakhney, A. I. Senkevich, T. N. Bondarenko, and V. D. Borisenko, Phys. Rev. B **63**, 075106 (2001).
[32] V. V. Nemoshkalenko, V. N. Uvarov, S. V. Borisenko, A. I. Senkevich, and T. N. Bondarenko, J. Electron Spectrosc. Relat. Phenom. **88–91**, 385 (1998).
[33] C. Heremans, B. J. Wuensch, J. K. Wuensch, J. K. Staick, and E. Prince, J. Solid State Chem. **117**, 108 (1995).
[34] J. G. Gibbons, Proc. IEEE **60**, 1062 (1972).
[35] W. J. Weber, R. C. Ewing, and L. M. Wang, J. Mater. Res. **9**, 688 (1994).
[36] W. J. Weber, J. Mater. Res. **5**, 2687 (1990).
[37] S. X. Wang, L. M. Wang, and R. C. Ewing, Phys. Rev. B **63**, 024105 (2001).
[38] W. J. Weber, Nucl. Instrum. Methods Phys. Res. B **166**, 98 (2000).
[39] S. X. Wang, L. M. Wang, and R. C. Ewing, in *Atomistic Mechanisms in Beam Synthesis and Irradiation of Materials*, edited by J. C. Barbour, S. Roorda, D. Ila, and M. Tsujioka, MRS Symposia Proceedings No. 504 (Materials Research Society, Pittsburgh, 1998), p. 165.
[40] A. Meldrum, L. A. Boatner, and R. C. Ewing, Phys. Rev. B **56**, 13 805 (1997).
[41] W. J. Weber, R. Devanathan, A. Meldrum, L. A. Boatner, R. C. Ewing, and L. M. Wang, in *Microstructural Processes in Irradiated Materials* (Ref. 11), p. 367.
[42] G. Y. Adachi and N. Imanaka, Chem. Rev. (Washington, D.C.) **98**, 1479 (1998).
[43] S. Kramer, M. Spears, and H. L. Tuller, Solid State Ionics **72**, 59 (1994).
[44] P. K. Moon and H. L. Tuller, in *Solid State Ionics*, edited by G. Nazri, R. A. Huggins, and D. F. Shriver, MRS Symposia Proceedings No. 135 (Materials Research Society, Pittsburgh, 1989), p. 149.
[45] K. E. Sickafus, L. Minervini, R. W. Grimes, J. A. Valdez, M. Ishimaru, F. Li, K. J. Meclellan, and T. Hartmann, Science **289**, 748 (2000).
[46] A. Meldrum, C. W. White, V. Keppens, L. A. Boatner, and R. C. Ewing, Phys. Rev. B **63**, 104109 (2001).
[47] B. J. Wuensch, K. W. Eberman, C. Heremans, E. M. Ku, P. Onnerud, E. M. Yeo, S. M. Haile, J. K. Stalick, and J. D. Jorgensen, Solid State Ionics **129**, 111 (2000).